

RSC Advances



This is an *Accepted Manuscript*, which has been through the Royal Society of Chemistry peer review process and has been accepted for publication.

Accepted Manuscripts are published online shortly after acceptance, before technical editing, formatting and proof reading. Using this free service, authors can make their results available to the community, in citable form, before we publish the edited article. This *Accepted Manuscript* will be replaced by the edited, formatted and paginated article as soon as this is available.

You can find more information about *Accepted Manuscripts* in the [Information for Authors](#).

Please note that technical editing may introduce minor changes to the text and/or graphics, which may alter content. The journal's standard [Terms & Conditions](#) and the [Ethical guidelines](#) still apply. In no event shall the Royal Society of Chemistry be held responsible for any errors or omissions in this *Accepted Manuscript* or any consequences arising from the use of any information it contains.

Facile laser-assisted synthesis of inorganic nanoparticles covered by carbon shell with tunable luminescence

Raúl García-Calzada,[†] Marina Rodio,[‡] Komal Bagga,^{‡,c} Romuald Intartaglia,^{*‡} Paolo Bianchini,[‡] Vladimir S. Chirvony,^{*†} Juan P. Martínez-Pastor[†]

[†]*UMDO - Unidad Asociada a CSIC-IMM, Instituto de Ciencias de los Materiales, Universidad de Valencia, PO Box 22085, 46071 Valencia, Spain*

[‡]*Nanophysics, Istituto Italiano di Tecnologia, via Morego, 30, 16163 Genova, Italy*

^c*Advanced Processing Technology Research Centre, School of Mechanical & Manufacturing Engineering, Dublin City University, Ireland.*

*To whom correspondence should be addressed:

E-mail: romuald.intartaglia@iit.it
vladimir.chirvony@uv.es

Abstract

We report on a one-step strategy at ambient conditions for the production of hybrid inorganic core/carbon shell nanoparticles by means of pulsed laser ablation of inorganic targets (LiNbO₃, Au, Si) in hydrocarbon liquids, such as toluene and chloroform. The core of these spherical nanoparticles consists of the target material, whereas the shells are carbon structures (multilayer graphite-type carbon and amorphous carbon), which are formed due to thermal decomposition of the organic liquid being in contact with hot inorganic nanoparticles ejected from a bulk target. The carbon shells emit photoluminescence in blue-green spectral regions and the found luminescence, which demonstrates dependence of the luminescence band maximum on the excitation wavelength, is analogous to the one observed for the so-called “carbon dots”.

1. Introduction

After the first publication discovering the outstanding visible luminescence properties of the so called “carbon dots” [1] an avalanche growth of the number of publications on luminescent carbon nanomaterials is observed [2-4]. These new carbonaceous materials are characterized by high optical absorptivity, high photoluminescence quantum yield (PL QY), chemical stability, biocompatibility, and low toxicity [5]. Besides, practically all types of CDs, as well as some of the luminescent graphene (oxide) nanodots [6-8], exhibit the dependence of the PL band position on the excitation wavelength, so that the PL can be tuned practically over all visible spectrum. Important is also to mention that really high values of the PL QY of CDs (up to 0.80) [4] are achieved only after special passivation and functionalization of their surface. Although the origin of CDs PL is still a matter of debate (see, for example, [4]), in the last years it became commonly accepted that surface states are involved in the PL [9-12].

The carbon dots are usually supposed to be used in biomedicine [5] or in chemical catalysis [13, 14]. Only very recently publications have appeared in which these new materials are considered as the candidates for use in photonics and optoelectronics [15]. Such a disproportion seems to be quite logical since carbon dots are normally produced as a suspension of nanometer-size plain graphitic sheets consisting of a few graphene monolayers. We believe that these carbonaceous nanostructures could find much wider applications in solid-state photonics and optoelectronics devices in case they are formed on underlying solid-state structures.

In this paper, we propose a laser based approach, namely pulsed laser ablation in liquid (PLAL) for a synthesis of such hybrid structures containing luminescent graphitic layers deposited on solid-state materials. In the last decade, PLAL has emerged as an appealing alternative approach to generate a wide range of nanomaterials [16-19] mainly due to the simplicity of the method. The main advantages of the technique include the green synthesis without chemical agents [16], the production of ligand-free nanoparticles [17], performed at ambient conditions, the versatility that allows *in situ* manipulations [20] and the high production yield [21]. Recently, it has been reported that the synthesis of nanomaterials in organic solvents can influence the composition and structure of the products [22-25].

In the present work we report on a new luminescent hybrid nanomaterial, which is produced by pulsed laser ablation of an inorganic solid target in an organic (hydrocarbon) liquid. The material is fabricated in the form of spherical nanoparticles (NPs) of the core/shell structure, where the inorganic core is produced by laser ablation of the target material, whereas the luminescent shell is a carbon structure (such as multilayer graphite or amorphous carbon), which is formed on the inorganic core surface due to thermal decomposition of a hydrocarbon liquid being in contact with hot core nanoparticle. The carbon shell is shown to exhibit excitation-wavelength dependent emission in the visible spectral region similarly to “classical” CDs.

2. Experimental details

We used a 128°-y cut LiNbO₃ wafer (Cstech), a gold film of 99.99% purity (Goodfellow Cambridge Ltd.), and a Si (100) p-type 20-30 ohm·cm wafer (ITME) as laser ablation targets. Spectral grade toluene and chloroform (Aldrich) were used as liquids to perform pulsed PLAL process. A Q-switched pulsed Nd:YAG laser (Spectra-Physics Quanta-Ray) generating 355 nm pulses of 10 ns duration with a repetition rate of 30 Hz was used to ablate different targets in liquids. The ablation pulse energy was fixed in all the experiments to about 20 mJ per pulse. The PLAL procedure consisted in expose of a solid target, which is immersed into a liquid in a vessel, to laser irradiation (usually during 5 minutes). The diameter of a laser spot on a sample was around 800 μm. The thickness of a liquid over the target was 5 mm. The vessel containing the liquid and the target was rotated during PLAL process to achieve more uniform irradiation over the target surface. The PLAL process was performed with keeping constant all controllable parameters (liquid layer thickness, pulse energy, vessel rotation velocity and laser beam configuration).

The PL spectra of the PLAL-produced suspensions were measured using a spectrofluorometer (FluoroMax-4, Horiba Jobin Yvon). The Raman characterization of dried PLAL products deposited on Si wafer was done using a laser excitation wavelength of 632 nm. The fluorescence microscopy has been performed by a Nikon confocal microscope (A1sp, Nikon Instruments, Japan) on suspensions of NPs dried on glass. We acquired several confocal images exciting both at 405 or 488 nm and collecting the PL in the spectral ranges 450-600 nm or 500-550nm, respectively. We

used a 60x 1.4 NA objective lens and a pixel dwell time of 52 μ s. TEM and HRTEM images were obtained with a Tecnai G² instrument operated at 100 kV. The preparation of the specimens was done by dropping a colloidal suspension over carbon-coated TEM copper grids. After complete evaporation of the liquids on air at room temperature the samples were transferred onto the electron microscope.

Dynamic Light Scattering (DLS) was performed using a Zetasizer Nano ZS90 (Malvern, USA) equipped with a 4.0 mW He-Ne laser operating at 633 nm and an Avalanche photodiode detector. Measurements were made at 25 °C on nanoparticles solutions. The values were determined using the Smoluchowsky approximation and were estimated as the average of three repeated measurements.

3. Results and Discussion

Studying the suspensions of nanostructures formed by a nanosecond laser ablation of solid targets (LiNbO₃, Si, Au) in organic liquids, we have found that, independently on a target used, the suspensions produced in toluene or chloroform exhibit PL. Figure 1 shows the confocal microscope images of the luminous materials produced by PLAL processing of LiNbO₃ target in toluene (a) and chloroform (b) as well as by PLAL of Au target in toluene (c) and CHCl₃ (d).

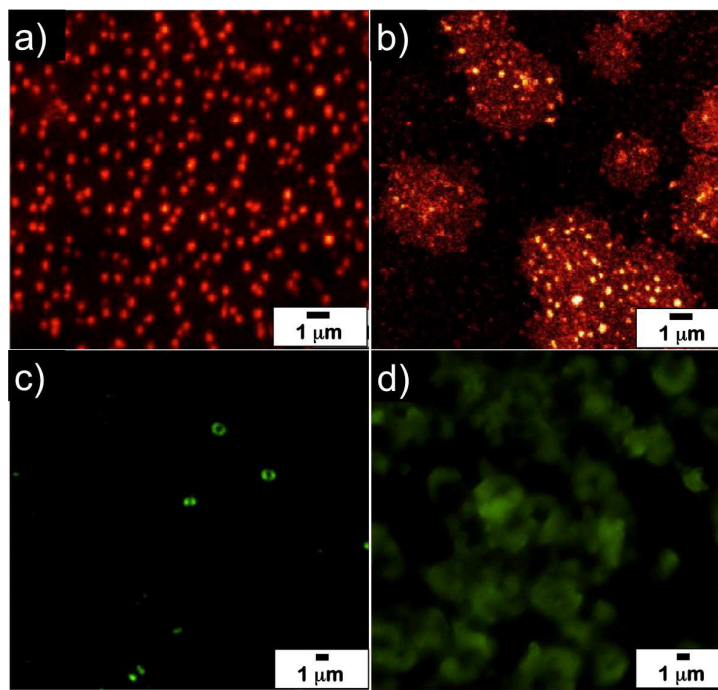


Figure 1. Confocal microscopy images of NPs obtained by PLAL of LiNbO₃ target in toluene (a) and CHCl₃ (b) shown in red false colours and of Au NPs obtained by PLAL of Au target in toluene (c) and CHCl₃ (d) shown in green false colours.

As one can see in Fig. 1, the emission is spotted. Given that LiNbO₃ and Au are not luminescent materials, clearly we should associate the origin of the PL with carbon byproducts obtained during the PLAL process in organic liquids. It is interesting to note that the spatial distribution of the emission in the images of Fig. 1a, 1c from one side and 1b, 1d from another side are different: in case of PLAL in toluene (1a, c) practically all the emitted light comes from isolated NPs, whereas in case of PLAL in CHCl₃ the formation of a few μm agglomerates is clearly observed with emitted light coming not only from NPs but also from the regions between them (“luminous clouds”). PLAL of Si target in the same two solvents results in confocal luminescence images similar to those presented in Fig. 1 (not shown).

To understand what structures are responsible for the detected PL, the morphology of nanostructures produced by PLAL in toluene and chloroform was studied using TEM and HRTEM techniques. In Figs. 2 and 3 we show the results obtained with LiNbO₃ as a target. Qualitatively similar HRTEM data were obtained in case of Si and Au targets (not shown).

In order to get insight of the morphology and structure of the luminescent product, conventional TEM and HR TEM analysis were performed. Analysis of TEM and HRTEM images of the LA products shows that, under the PLAL conditions used (time of ablation, excitation wavelength and energy), the laser ablation of LiNbO₃ target immersed in toluene or chloroform yields perfect crystalline spherical LiNbO₃ NPs with diameters in a wide interval between 10 and 200 nm (see Fig. 2). (Obtaining narrow size distribution of the ablation-produced NPs was not the aim of the present work.)

As one can see in Fig. 2, the nanostructures obtained by ablation of the target in toluene from one side and in chloroform – from another side, are significantly different. Indeed, individual NPs coated by a shell are formed in case of toluene (the shell is clearly visible in Fig. 2c), whereas PLAL in chloroform results in formation of chain-like agglomerates consisting of both LiNbO₃ NPs as well as of carbon-based NPs (the latter are visible as less dense objects in Fig. 2b). As Fig. 2d shows, the entire structure of the synthesized agglomerates is wrapped in an amorphous material, which can be identified as amorphous carbon (a-C). It should be noted that the

structures described in Fig. 2 are similar to those observed earlier as a result of PLAL of a gold target in liquids: In particular, in Ref. 26 the authors observed formation of multilayer carbon (graphitic) shell around gold NPs after PLAL in toluene, whereas in Ref. 27 the authors found, as a result of laser ablation of Au target in chloroform, a formation of chain-like aggregates consisting mainly of amorphous carbon. It is worth to note, however, that in both publications no any information was presented about PL properties of PLAL products.

The found different structure of PLAL products obtained in toluene (individual NPs) and chloroform (NPs aggregates) is unambiguously confirmed by the results of Dynamic Light Scattering experiments (see Fig. S1): ~ 100 nm average diameter is obtained in the former case and ~ 1 μm diameter in the latter.

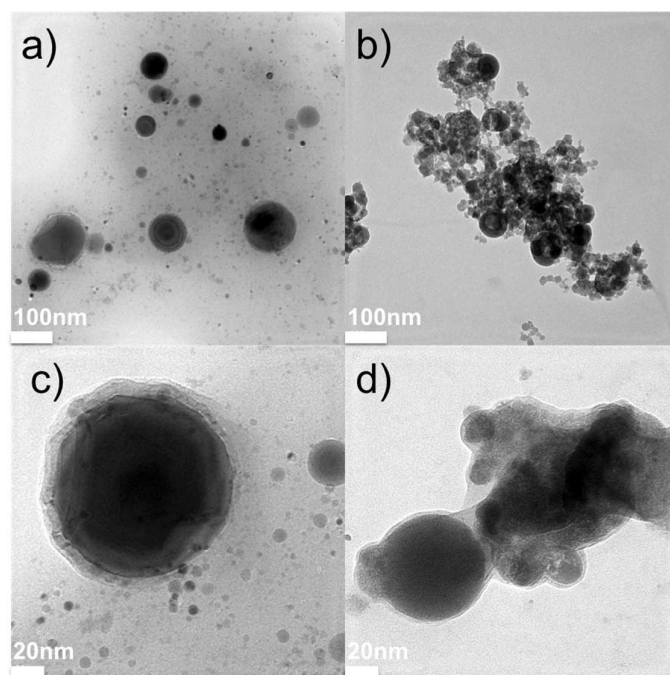


Figure 2. TEM image of nanostructures obtained by laser ablation of LiNbO_3 target in toluene (a, c) and in chloroform (b, d). Scale bars are 100 nm (a, b) and 20 nm (c, d).

Complementary to TEM, HRTEM analysis reveals that the PLAL product has highly crystalline structure. HRTEM images (Fig. 3) shows that, along with highly crystalline LiNbO_3 NPs, which are characterised by a 2.58 \AA distance between diffraction fringes (that corresponds to the (020) orientation of the crystalline core, see Fig. 3A), multilayer shells are formed around LiNbO_3 NP surface. The shells

contain only amorphous phase (a-C) in case of ablation in chloroform (Fig. 3B), whereas in case of toluene one can identify a carbon multilayer (CML) structure deposited on LiNbO₃ NP surface and covered then by an amorphous shell. Interlayer distance for this CML is found to be 3.45 Å (Fig. 3A) that corresponds to bulk graphite interplanar distance.

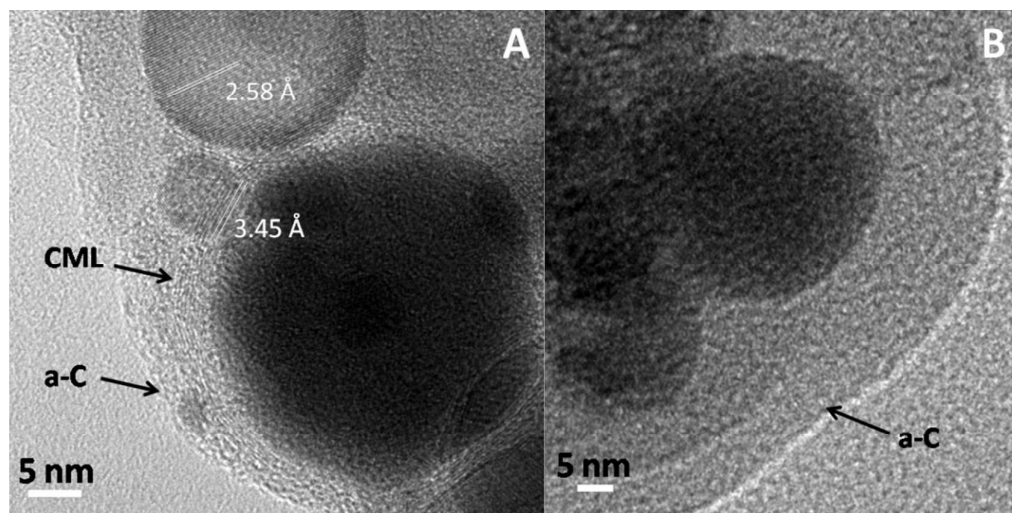


Figure 3: HRTEM images of nanostructures obtained by laser ablation of LiNbO₃ target in toluene (A) and in chloroform (B).

Similarly to the case of LiNbO₃ target, ablation of Au and Si targets in toluene resulted in formation of multilayer graphitic shells around target NPs, whereas in case of ablation in CHCl₃ only a-C material is detected (not shown).

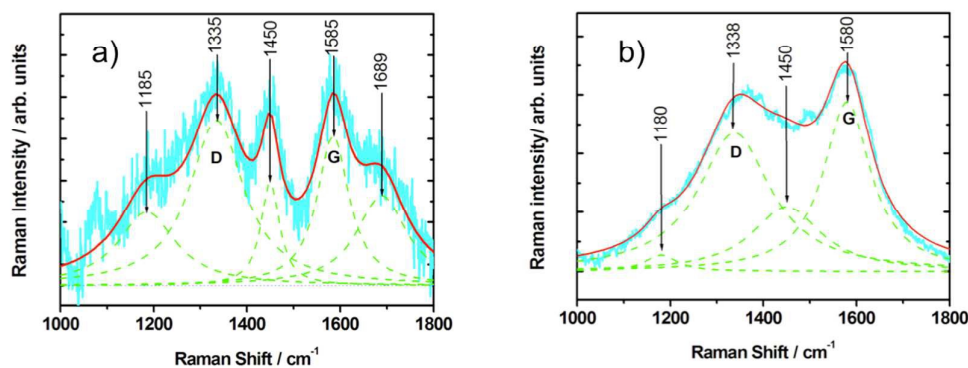


Figure 4. Raman spectra of products of PLAL processing of LiNbO₃ target in toluene (a) and chloroform (b). The noisy lines (in cyan colour) correspond to the experimental spectra, the red solid lines represent the result of the experimental spectrum modelling by Lorentzian

contours; the individual Lorentzian contours are shown by green dash lines. Positions of the contour maxima are also indicated.

In order to obtain additional information on the origin of the products of the solid targets laser ablation in the two organic liquids, we have also investigated their Raman spectra in the 1000-1800 cm^{-1} region. The Raman spectra are presented in Fig. 4 (for the case of LiNbO_3 target in toluene) and Figs. S2 – S3 for other cases.

In all cases the Raman spectra consisted of several very broad superimposed bands. Fitting by Lorentzian contours enabled us to select four main bands, which manifest themselves in each of the six measured spectra: these are three intensive bands with clearly visible maxima at ~ 1340 , ~ 1450 and $\sim 1580 \text{ cm}^{-1}$ as well as one less intensive band with the maximum near 1150-1180 cm^{-1} visible in the experimental Raman spectra as a shoulder.

Since all target materials (LiNbO_3 , Si and Au) do not exhibit any pronounced Raman lines in the investigated spectral region, one can suggest that the observed Raman bands belong to those PLAL products, which are produced due to decomposition of organic liquids in course of PLAL process. Indeed, it is well known that the Raman spectra of all carbons show several common features in the 800 – 2000 cm^{-1} region, the so-called *G* and *D* peaks, which lie at around 1560 and 1360 cm^{-1} for visible excitation, and the *T* peak, seen only for UV excitation at around 1060 cm^{-1} [28]. The *G* and *D* peaks are known to be due to sp^2 sites only [28]. The *G* peak is due to the bond stretching of all pairs of sp^2 atoms in both rings and chains [29]. The *D* peak is due to the breathing modes of sp^2 atoms in rings. Therefore, the observation of *D* and *G* bands as main lines in our spectra unambiguously evidence in favor of a presence of sp^2 carbon structures. Without special investigations, including multiwavelength Raman studies [28], impossible to evaluate relative contributions of sp^2 and sp^3 carbon in the laser ablation products and conclude about relative contributions of different morphological carbon structures (disordered carbon, amorphous carbon, graphite-like carbon and others). We can only note that large spectral width of the observed *G* and *D* bands evidences in favour of the presence of highly disordered graphitic structures [29].

An interpretation of the intense band at 1450 cm^{-1} requires more detailed analysis. Very often this Raman band around 1450 cm^{-1} , which usually appears together with the one near 1150 cm^{-1} in case of nanocarbon materials, is assigned to

the “phonon frequencies at K and M points of graphite equivalent Brillouin zone” [30]. However, the argumentation presented in Ref. 31 convinced us that the ~ 1150 - and ~ 1450 cm^{-1} peaks should be assigned to the ν_1 and ν_3 modes of trans-polyacetylene (trans-PA) molecules [32]. These modes are roughly sum and difference combinations of C=C chain stretching and CH wagging modes. Since Raman cross section of polyacetylene is very high as compared to G and D bands of graphite [31], the relative amount of trans-PA in the PLAL products may be very small.

Finally, the very broad band, which exhibits its maximum at about 1690 cm^{-1} in some of the Raman spectra of the obtained products can be interpreted as a molecular C=C symmetric stretching vibration. Indeed, as indicated in the literature, this vibration is strong in Raman spectra and can be detected in $1500 - 1900$ cm^{-1} region [33]. Concerning the formation of C=C bonds even in the case of use of CHCl_3 as ablation medium we expect that the very high temperature conditions of the laser ablation experiments can be responsible for this. Indeed, there are indications in the literature that, in case of high-temperature chloroform pyrolysis ($>850^\circ\text{C}$), C_2H_4 is one of the major products [34].

All photoluminescence data obtained can be classified as follows. PL spectra of suspensions produced by PLAL of all used targets in toluene are similar. The main characteristic of these spectra is a dependence of the luminescence band on excitation wavelength, and more exactly, a monotonous shift of the PL band maximum to the long wavelength side, from 350 to 570 nm, when increasing the excitation wavelength from 300 to 500 nm, respectively. A typical example of such behaviour is presented in Fig. 5 for the case of the suspension obtained by PLAL of LiNbO_3 target in toluene.

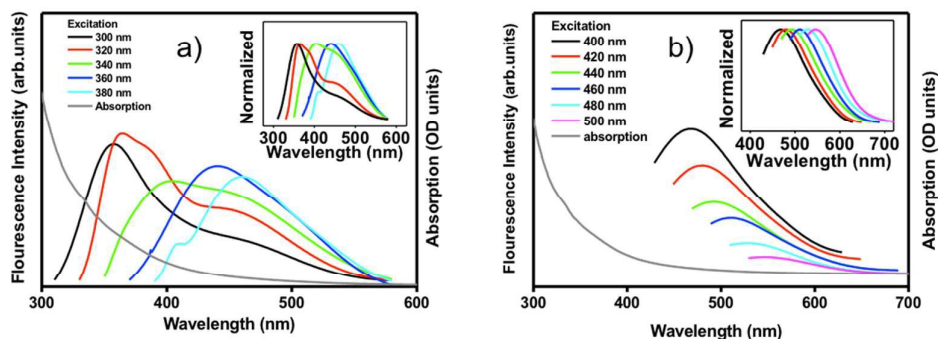


Figure 5. PL spectra of a suspension of NPs produced by PLAL of LiNbO₃ target in toluene. Excitation of the PL was at 300 to 380 nm (a) and at 400 to 500 nm (b). Insets show normalized PL spectra. Absorption spectrum is also shown (solid grey line).

As one can see in Fig. 5, excitation in 300-340 nm interval results in two-band photoluminescence, the bands maxima are near 360 and 450 nm. Starting from 360 nm excitation the further shift of the excitation wavelength from blue to the green side is accompanied by the single PL band shift towards long wavelengths without modification of the band spectral shape. PL quantum yield of the suspension produced by PLAL of LiNbO₃ in toluene was about 0.01 under 360 nm excitation using quinine bisulfate in 0.10 N H₂SO₄ as a reference (PL quantum yield 0.53) [35]. Similar PL quantum yield values are usually published in literature for as-synthesized CDs not subjected to additional passivation post-treatments. (Comprehensive photophysical investigation of the luminescent products is now in progress and the results obtained will be published elsewhere.)

Contrary to the behaviour of PL spectra of suspensions produced in toluene, suspensions in chloroform either do not demonstrate any (in case of LiNbO₃ and Au targets) or demonstrate weak (in case of Si target) dependence of spectral position of their PL band maxima on excitation wavelength. Typical example of such behaviour is presented in Fig. S4. As one can see from this figure, excitation at 300-400 nm results in appearance of a single PL band with the maximum near 450 nm, and the following shift of the excitation to 500 nm is not accompanied by the appearance of a long wavelength-shifted PL band with a distinct band maximum. Instead, only tail of the previous very broad 450 nm PL band is detected.

Finally, in case of the suspension produced by PLAL of Si target in chloroform only a moderate shift of the PL band maximum is observed from about 500 to 550 nm when excitation shifts from 300 to 500 nm (see Fig. S5).

When viewing the Figs. S4 and S6 one can observe an interesting difference in absorption spectra of the suspensions produced by PLAL of a gold target in chloroform (Fig. S4) and in toluene (Fig. S6). Indeed, in case of chloroform a distinct plasmonic band is observed with the maximum at 550 nm belonging to Au NPs, whereas the corresponding maximum is absent in case of Au NPs produced in toluene. We suggest that two reasons may be responsible for such effect. First, in our experiments the average size of Au NPs produced in toluene is less than 5 nm, and it has been shown earlier that for very small (2-3 nm diameter) Au NPs plasmonic band

is not observed [36,37]. On the other hand, Amendola et al. have shown [26] that the formation of graphitic multilayer structure on Au NP surface quenches plasmonic absorption band that can be ascribed to the formation of covalent bonds at the surface exhausting/localizing free electrons at the metal NP [38].

We would like to conclude the consideration of PL properties of the produced hybrid nanoparticles with a discussion on the nature of photoluminescence of CDs in general because it can shed light on the PL origin in our structures. In general, all proposed mechanisms of CDs photoluminescence can be divided onto two parts: (1) the mechanisms considering PL as a result of radiative deactivation (due to electron-hole recombination) of excitonic (collective) electronic states delocalized over a nanocrystal, and (2) the mechanisms related to radiative deactivation of surface states localized on specific chemical (functional) groups. Although in many earlier works explanation of CDs PL was related with the mechanism (1) [39-44], unambiguous data appeared last years that weight the scale on behalf of the mechanism (2). In particular, very convincing results on PL origin in CDs were obtained in Ref. 45, where photoluminescence of nanodiamonds was investigated. It is well known that “ideal” bulk diamond do not exhibit any visible PL and only formation of crystallographic defects in the diamond crystal structure, where each C atom is sp^3 -hybridized, may result in appearance of PL in the visible spectral region. In case of nanodiamonds, due to enormously increased surface-to-volume ratio, the role of surface defect states in formation of physical-chemical and photophysical properties of the nanostructures drastically increases. It was shown [45] that, in spite of the fact that nanodiamonds are distinctly different from carbon quantum dots (with their essential contribution of sp^2 -hybridized carbon) from the point of view of their crystalline and electronic structure, nanodiamond colloids exhibit strong visible excitation-dependent fluorescence. This effect is unrelated to the size (i.e. electron confinement) effect and can be explained by a presence of several types of localized surface states related with functional groups residing on the nanodiamonds, such as hydroxyl OH, carbonyl C=O, and carboxyl COOH groups [45].

Similar conclusions about the origin of visible PL in few-layer graphite-type structures were done in many other publications. Thus, in Ref. 9, green luminescence in differently synthesized an possessing different morphology CDs and graphene oxide QDs were assigned to special edge states consisting of several carbon atoms on the edge of carbon (graphite) backbone bound with carbonyl C=O or carboxyl

COOH groups. In Ref. 10 the PL of CDs was assigned to the presence of oxygen-containing C=O and -OH groups on CD surface chemically bound to graphitic structure. At last, it is demonstrated in the Ref. 11 on the basis of careful optical investigations that the so-called “carbon dots” are not “quantum dots” and are not even “dots”: due to the presence of electronic anisotropy of the corresponding optical emission they cannot be considered as “dots”, objects of zero dimension. The authors showed also that the CDs fluorescence response is not collective and represents a composition of individual emitters [11]. According to the presented results, the so-called “carbon dots” are considered in Ref. 11 as nano-sized clusters assembling individual fluorophores, which are formed on the particle surface.

On the basis of the above literature data, the observed complex dependence of the PL spectra on excitation photon energy (Fig. 5), when two PL bands with maxima at about 350 and 450 nm are detected under 300-330 nm excitation and only the latter inhomogeneously broadened PL band is detected when excitation is realised in 360-550 nm interval, may be explained, in general terms, as follows [11]. Different functional groups (-OH, C=O, COOH) bound to graphitic matrix form different luminescent centres, so that illumination by UV light (300-330 nm) preferably excites luminescent centres containing -OH groups, which possesses PL with a maximum near 350 nm. The illumination by blue-green light excites mainly the centres containing C=O and COOH groups, which demonstrate inhomogeneously broadened PL in green and even yellow regions. We suggest that the absence of the blue PL band in case of LA in chloroform may be simply related with the fact that the content of hydrogen in CHCl_3 is much lower than that in toluene (C_6H_6) that prevents the formation of OH-related luminescent centres in a sufficient concentration.

Conclusion

In conclusion, we have reported on a novel method for the fabrication of luminescent hybrid carbon-inorganic nanoparticles using one-pot laser based strategy at ambient conditions. The material is in the form of nanoparticles of the core/shell structure, where the core is an inorganic spherical nanoparticle produced by laser ablation from the target material, whereas the luminescent shell is a carbon-based (graphite-type multilayer or amorphous carbon) structure. Studies reveal an excitation-wavelength dependent carbon-based multicolour emission in the visible spectral region similarly

to carbon dots. Our method is versatile and allows the generation of a large variety of core/shell structure by selecting properly the target material used for the ablation. We also suggest that an analogous strategy can be used for deposition of graphitic layers on preformed NPs immersed into an organic liquid like toluene and irradiated by intensive laser pulses, which are well absorbed by the NPs to increase their temperature sufficiently for the liquid decomposition. The proposed approach opens the route towards fabrication of luminescent solid-state materials, which can find applications in photonic devices due to their high refractive index, high mechanical hardness, possibility to use plasmonic effects in case of metallic core etc.

Acknowledgments

This work was supported through the Spanish MCINN (project TEC2011-29120-C05-01), Generalitat Valenciana (Grant PROMETEOII/2014/059) and the EU Grant EU-FP7 NMP-246331 (NanoPV). We thank the Nikon Imaging Center at the Fondazione Istituto Italiano di Tecnologia for help with light microscopy.

References

1. Y.-P. Sun, B. Zhou, Y. Lin, W. Wang, K. A. S. Fernando, P. Pathak, M. J. Meziani, B. A. Harruff, X. Wang, H. Wang, P. G. Luo, H. Yang, M. E. Kose, B. Chen, L. M. Veca and S.-Y. Xie, *J. Am. Chem. Soc.* 2006, **128**, 7756.
2. S. N. Baker, G. A. Baker, *Angew. Chem. Int. Ed.* 2010, **49**, 6726.
3. H. Li, Z. Kang, Y. Liu and S. T. Lee, *J. Mater. Chem.* 2012, **22**, 24230.
4. S. Zhu, Q. Meng, L. Wang, J. Zhang, Y. Song, H. Jin, K. Zhang, H. Sun, H. Wang and B. Yang, *Angew. Chem. Int. Ed.* 2013, **52**, 3953.
5. Z. Li, Q. Sun, Y. Zhu, B. Tan, Z. P. Xu and S. X. Dou, *J. Mater. Chem. B* 2014, **2**, 2793.
6. D. Pan, J. Zhang, Z. Li and M. Wu, *Adv. Mater.* 2010, **22**, 734.
7. S. Zhu, J. Zhang, X. Liu, B. Li, X. Wang, S. Tang, Q. Meng, Y. Li, C. Shi and R. H. B. Yang, *RSC Advances* 2012, **2**, 2717.
8. X. Zhang, S. Wang, M. Liu, B. Yang, L. Feng, Y. Ji, L. Tao and Y. Wei, *Phys. Chem. Chem. Phys.* 2013, **15**, 19013.
9. L. Wang, S.-L. Zhu, H.-Y. Wang, S. N. Qu, Y.-L. Zhang, J.-H. Zhang, Q.-D. Chen, H.-L. Xu, W. Han, B. Yang and H.-B. Sun, *ACS Nano* 2014, **8**, 2541.
10. S. Ghosh, A. M. Chizhik, N. Karedla, M. O. Dekaliuk, I. Gregor, H. Schuhmann, M. Seibt, K. Bodensiek, I. A. Schaap, O. Schulz, A. P. Demchenko, J. Enderlein and A. I. Chizhik, *Nano Lett.* 2014, **14**, 5656.
11. M. O. Dekaliuk, O. Viagin, Yu. V. Malyukin and A. P. Demchenko, *Phys. Chem. Chem. Phys.* 2014, **16**, 16075.
12. S. Cushing, M. Li, F. Huang and N. Wu, *ACS Nano* 2014, **8**, 1002.
13. P. Mondal, K. Ghosal, S. K. Bhattacharyya, M. Das, A. Bera, D. Ganguly, P. Kumar, J. Dwivedi, R. K. Gupta, A. A. Martí, B. K. Gupta and S. Maiti, *RSC Adv.*, 2014, **4**, 25863.
14. D. Dey, T. Bhattacharya, B. Majumdar, S. Mandani, B. Sharma and T. K. Sarma, *Dalton Trans.*, 2013, **42**, 13821-13825
15. X. Han, S. Zhong, W. Pan and W. Shen, *Nanotechnology* 2015, **26**, 065402.
16. V. Amendola and M. Meneghetti, *Physical chemistry chemical physics : PCCP*, 2009, **11**, 3805-3821.
17. R. Intartaglia, G. Das, K. Bagga, A. Gopalakrishnan, A. Genovese, M. Povia, E. Di Fabrizio, R. Cingolani, A. Diaspro and F. Brandi, *Physical chemistry chemical physics : PCCP*, 2013, **15**, 3075-3082.
18. V. S. Vendamani, S. Hamad, V. Saikiran, A. P. Pathak, S. Venugopal Rao, V. V. Ravi Kanth Kumar and S. V. S. Nageswara Rao, *J Mater Sci*, 2015, **50**, 1666-1672.
19. S. Hamad, G. K. Podagatlapalli, V. S. Vendamani, S. V. S. Nageswara Rao, A. P. Pathak, S. P. Tewari and S. Venugopal Rao, *The Journal of Physical Chemistry C*, 2014, **118**, 7139-7151.

20. K. Bagga, A. Barchanski, R. Intartaglia, S. Dante, R. Marotta, A. Diaspro, C. L. Sajti and F. Brandi, *Laser Phys. Lett.*, 2013, **10**, 065603.
21. R. Intartaglia, K. Bagga and F. Brandi, *Optics express*, 2014, **22**, 3117-3127.
22. V. Amendola and M. Meneghetti, *Physical Chemistry Chemical Physics*, 2013, **15**, 3027-3046.
23. R. Intartaglia, K. Bagga, A. Genovese, A. Athanassiou, R. Cingolani, A. Diaspro and F. Brandi, *Physical chemistry chemical physics : PCCP*, 2012, **14**, 15406-15411.
24. P. G. Kuzmin, G. A. Shafeev, V. V. Bukin, S. V. Garnov, C. Farcau, R. Carles, B. Warot-Fontrose, V. Guieu and G. Viau, *The Journal of Physical Chemistry C*, 2010, **114**, 15266-15273.
25. C.-C. Huang, K.-Y. Chuang, C.-J. Huang, T.-M. Liu and C.-S. Yeh, *The Journal of Physical Chemistry C*, 2011, **115**, 9952-9960.
26. V. Amendola, G. A. Rizzi, S. Polizzi and M. Meneghetti, *J. Phys. Chem. B* 2005, **109**, 23125.
27. K. Siskova, J. Pfliegera and M. Prochazka, *Appl. Surf. Sci.* 2010, **256**, 2979.
28. A. C. Ferrari and J. Robertson, *Phys. Rev. B* 2001, **64**, 075414.
29. A. C. Ferrari and J. Robertson, *Phys. Rev. B* 2000, **61**, 14095.
30. F. Du, J. Yuan, M. Zhang, J. Li, Z. Zhou, Z. Li, M. Cao, J. Chen, L. Zhang, X. Liu, A. Gong, W. Xua and Q. Shao, *RSC Adv.* 2014, **4**, 37536.
31. A. C. Ferrari and J. Robertson, *Phys. Rev. B* 2001, **63**, 121405(R).
32. E. Ehrenfreund, Z. Vardeny, O. Brafman and B. Horovitz, *Phys. Rev. B* 1987, **36**, 1535.
33. Horiba,
<http://www.horiba.com/fileadmin/uploads/Scientific/Documents/Raman/bands.pdf>, (accessed April 2015).
34. Y.-S. Won, *Korean J. Chem. Eng.* 2012, **29**, 1745
35. K. Suzuki, A. Kobayashi, S. Kaneko, K. Takehira, T. Yoshihara, H. Ishida, Y. Shiina, S. Oishi and S. Tobita, *Phys. Chem. Chem. Phys.* 2009, **11**, 9850.
36. B. Palpant, B. Prével, J. Lermé, E. Cottancin, M. Pellarin, M. Treilleux, A. Perez, J. L. Vialle and M. Broyer, *Phys. Rev. B* 1998, **57**, 1963.
37. G. C. Lica, B. S. Zelakiewicz, M. Constantinescu and Y. Y. Tong, *J. Phys. Chem. B* 2004, **108**, 19896.
38. R. Abargues, P. J. Rodriguez-Canto, S. Albert, I. Suarez and J. P. Martínez-Pastor, *J. Mater. Chem. C* 2014, **2**, 908.
39. T. Gokus, R. R. Nair, A. Bonetti, M. Bohmler, A. Lombardo, K. S. Novoselov, A. K. Geim and A. C. Ferrari, *ACS Nano* 2009, **3**, 3963.
40. Y. M. Long, C. H. Zhou, Z. L. Zhang, Z. Q. Tian, L. Bao, Y. Lin and D. W.

- Pang, *J. Mater. Chem.* 2012, **22**, 5917.
41. H. Li, X. He, Z. Kang, H. Huang, Y. Liu, J. Liu, S. Lian, C. H. A. Tsang, X. Yang and S. T. Lee, *Angew. Chem., Int. Ed.* 2010, **49**, 4430.
 42. S. Srivastava and N. S. Gajbhiye, *ChemPhysChem* 2011, **12**, 2624.
 43. X. Wang, L. Cao, S. T. Yang, F. Lu, M. J. Meziani, L. Tian, K. W. Sun, M. A. Bloodgood and Y. P. Sun, *Angew. Chem. Int. Ed.* 2010, **49**, 5310.
 44. B. Zhu, S. Sun, Y. Wang, S. Deng, G. Qian, M. Wang and A. Hu, *J. Mater. Chem. C* 2013, **1**, 580.
 45. J. Xiao, P. Liu, L. Li and G. Yang, *J. Phys. Chem. C* 2015, **119**, 2239.